Available online at www.sciencedirect.com

Manufacturing Letters

Manufacturing Letters 44 (2025) 643–650

53rd SME North American Manufacturing Research Conference (NAMRC 53, 2025)

Prediction of residual stresses induced in turning – Influence of cutting tool geometry

Joel Rech[a]*, Sangil Han[a], Alexis Cavard[b], Marc Raffestin[a], Frédéric Valiorgue[a]

a University of Lyon, Centrale Lyon ENISE, LTDS UMR CNRS 5513, 58 Rue Jean Parot, 42000 Saint-Etienne, France
b MISUTECH, 74 Rue des aciéries, 42000 Saint-Etienne, France

* Corresponding author. Tel.: +33677098123; *E-mail address:* joel.rech@enise.fr

Abstract

It has long been recognised that machining processes induce residual stresses in machined surfaces. This article focuses on the longitudinal turning process of the martensitic stainless steel 15-5PH. The aim is to investigate the influence of tool geometry, specifically rake angle and edge sharpness, on surface residual stresses. Three turning tools were studied both experimentally and through numerical simulations using the MISULAB software. The results show that the geometry of the cutting tool does not significantly affect the residual stress state in the outer layer. On the contrary, edge radius and rake angle determine the thickness of the affected layer as well as the intensity of the compression peak below the outer layer. Cutting tools with a large edge radius and a small rake angle result in a thick affected depth, characterised by a deep compression peak below the outer layer. The trends observed experimentally are well predicted by the numerical simulations, providing new insights for the design of new cutting tools dedicated to the optimisation of the residual stress state.

Peer-review under responsibility of the scientific committee of the NAMRI/SME.
Keywords: turning; cutting tool geometry; residual stresses; numerical modeling

1. Introduction

It has been known for many years that machining processes induce residual stresses in the near-surface region. Residual stresses play an important role in the durability of mechanical components (fatigue, corrosion, etc.). Numerous review articles have addressed the influence of machining operations on the integrity of machined surfaces [1-4]. As reported by [4], cutting processes, involving high mechanical stresses, promote the generation of compressive stresses at the surface, while cutting processes characterized by a high concentration of energy lead to thermal mechanisms that result in tensile stresses. Unfortunately, these keynote papers have also highlighted that the generation of residual stresses is governed by complex, non-linear, and highly coupled thermal and mechanical phenomena. Although the turning process is one of the simplest to study, given the complexity of these phenomena, it is nearly impossible to intuitively predict a residual stress state. This is why many scientific articles have conducted experimental studies to understand the mechanisms of residual stress generation in turning.

This article will focus on the turning process, specifically on the influence of cutting tool geometry on the generation of residual stresses. Fig.1 shows the main parameters describing the geometry of a turning tool.

In the scientific literature, it is apparent that many authors have studied the influence of the corner radius R_ε [5-11]. This parameter is important for industry as it largely determines the generated surface roughness. Additionally, it is quite accessible for scientists since commercially available cutting tools generally come with a wide range of corner radii while keeping other parameters constant.

This article focuses solely on the influence of edge sharpness R_β and the rake angle γ_n. These parameters are much more complex to study. It is difficult to study them independently because commercially available cutting tools vary all these

Peer-review under responsibility of the scientific committee of the NAMRI/SME.

parameters simultaneously. Furthermore, custom-made tools are necessary if one wishes to conduct a study to examine these parameters separately. This is both challenging and costly. For this reason, a limited number of authors have studied the influence of these two parameters.

Some authors, such as [9-10,12-14] have examined the influence of cutting tool geometry in the context of turning hardened steels. The machining of aircraft engine parts in Inconel 718 has also been an area of application for these geometric parameters [6-8]. Other studies, such as that by [9], have examined the influence of edge sharpness R_β in the turning of 316L stainless steel. Additionally, there are numerous studies on the influence of tool wear [6,7,15], which also represents a form of local tool geometry variation (primarily a change in edge sharpness R_β and clearance angle α_n rather than rake angle γ_n). However, it is challenging to control these geometric parameters to draw broader conclusions about new tools.

All these studies have provided concrete information for specific industrial applications, but their conclusions are not generalizable for predicting the residual stress state in any longitudinal turning operation. Indeed, many studies [6,8,9,16] have focused on 2D orthogonal cutting, an interesting setup for scientific understanding of the mechanisms but difficult to translate into a 3D industrial context, such as longitudinal turning.

Moreover, studies conducted in 3D longitudinal turning [7,9,10,14] are valid only for a single machined material and a limited range of machining conditions. It is impossible to generalize these findings to another material or extrapolate to different machining conditions.

Thus, with the goal of generalizing the prediction of residual stresses induced by longitudinal turning operations, several authors have developed numerical simulations with different cutting tool geometries [6,8,11,16]. Unfortunately, these models only consider 2D orthogonal cutting configurations. Nevertheless, industrial software now exists, which allows for predicting the influence of a 3D longitudinal turning operation on the generated residual stress state. For instance, the MISULAB software is derived from the scientific work presented in the article [17].

It is now possible to combine both industrial longitudinal turning tests to experimentally analyze the residual stress state and simultaneously conduct a numerical sensitivity study to assess the ability of this software to predict the influence of these geometric tool parameters (edge sharpness R_β, rake angle γ_n).

Thus, the aim of this article is to present a dual study of the experimental sensitivity of the residual stress state generated by industrial cutting tools with different edge sharpness R_β and rake angles γ_n, as well as to numerically simulate these industrial machining configurations with a 3D model to evaluate the capability of these models to predict residual stresses in other geometric configurations in the future.

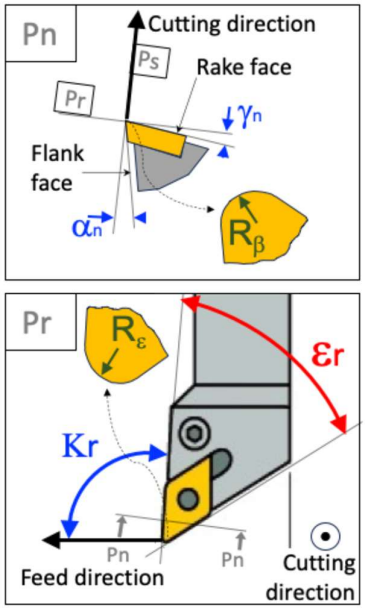

Fig.1. Geometrical parameters of a cutting tool in longitudinal turning.

2. Experimental tests

Longitudinal turning tests were performed on a CNC lathe, as shown in Fig.2. Several workpieces with a diameter of 80 mm, made of 15-5PH martensitic stainless steel (state H1025, hardness = 35 HRC; tensile strength = 1070 MPa; yield strength = 1000 MPa), were prepared.

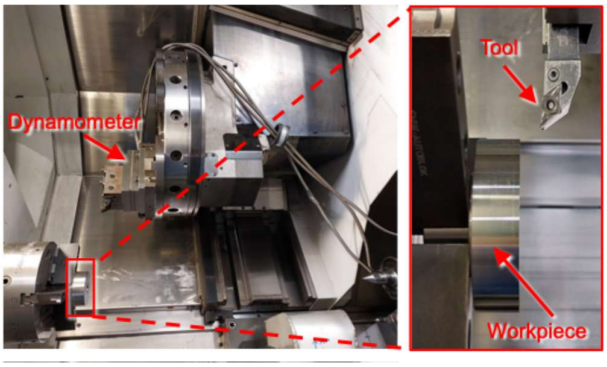

Fig.2. Experimental set-up for longitudinal turning.

Three carbide cutting inserts available on the market and designed for the longitudinal turning of 15-5PH steel were selected:

- DNMG 150608 (red color in the following tables and curves)
- DNMG 150408 (yellow)
- DCGT 11T308 (green)

Their geometric parameters were characterized using a confocal microscope, and the values are reported in Table 1. It can be observed that they mainly differ in their edge sharpness Rβ and rake angle γn, while other parameters, including the corner radius R_ε, remain almost constant. The DNMG 150608 insert (red) has a large edge sharpness R_β (around 63 µm), while the DNMG 150408 insert (yellow, around 35 µm) has an

intermediate value, and the DCGT 11T308 insert (green) has the smallest value, around 18 µm.

Regarding the rake angle γ_n, the DNMG 150608 insert (red) has a neutral rake angle (close to 0°), the DNMG 150408 insert (yellow) has an intermediate angle (around 6°), and the DCGT 11T308 insert (green) has the highest angle (around 20°). Fig.3 illustrates a schematic view of the local shape of the three inserts: the red insert is the most rounded tool, the green one is the sharpest, and the yellow one has an intermediate geometry.

Table 1. Geometrical characterization of cutting inserts.

	Corner radius R_ε (mm)	Angle ϵ_r (°)	Lead angle κ_r (°)	Edge sharp. R_β (mm)	Rake angle γ_n (°)	Clear. angle α_n (°)
DNMG150608	0.8	55	95	0.063	1.3	8
DNMG150408	0.8	55	95	0.035	6.6	7.4
DCGT11T308	0.8	55	95	0.018	20	6.4

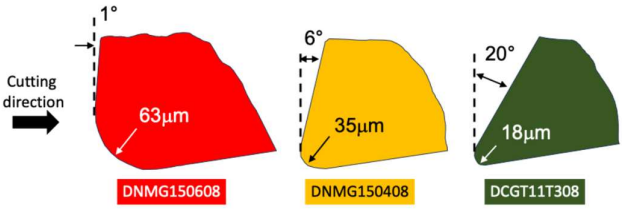

Fig.3. Schematic view of the local geometry of the 3 inserts.

The tests were conducted under dry conditions and with the following cutting parameters: a cutting speed V_c of 120 m/min with a feed rate f of 0.2 mm/rev and a depth of cut a_p of 0.2 mm.

A dynamometer was used to measure the cutting forces (F_c, F_p, F_a). Each cutting insert has been tested three times. Average experimental force values are reported in Table 2. As expected, the red insert resulted in the highest cutting and penetration forces, while the green insert produced the lowest values.

Table 2. Forces measured in longitudinal turning

	DNMG 150608	DNMG 150408	DCGT 11T308
Cutting Force, Fc (N)	133	120	94
Penetration Force, Fp (N)	146	107	40

As shown in Fig.4, residual stresses were assessed by the X-Ray diffraction method using an iXRD system by PROTO Company, a MG40 head equipped with a 2-mm diameter collimator and following the conditions used in Table 3. Electrolytic etching was applied successively at the same location to perform the measurement at different depths.

Fig.5 presents the three residual stress profiles for each of the three inserts (a total of 9 residual stress profiles). It can be observed that typical residual stress profiles for turning operations have been generated. The external layer shows a peak toward tension, while the subsurface is strongly compressed. The stress state then returns to the original stress in the bulk of the sample. These profiles are consistent with previous results from turning 15-5PH steel [17]. The natural deviation of residual stress is also observable. It can be noted that the residual stress on the external layer is significantly scattered in the circumferential direction, which has already been observed by [17].

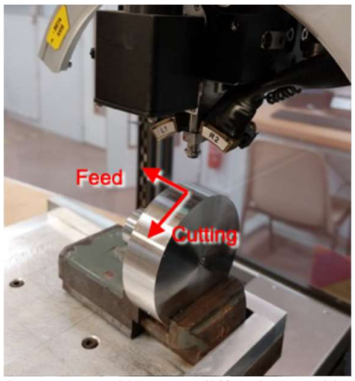

Fig.4. Specimen mounted in X-ray diffraction machine (Proto®).

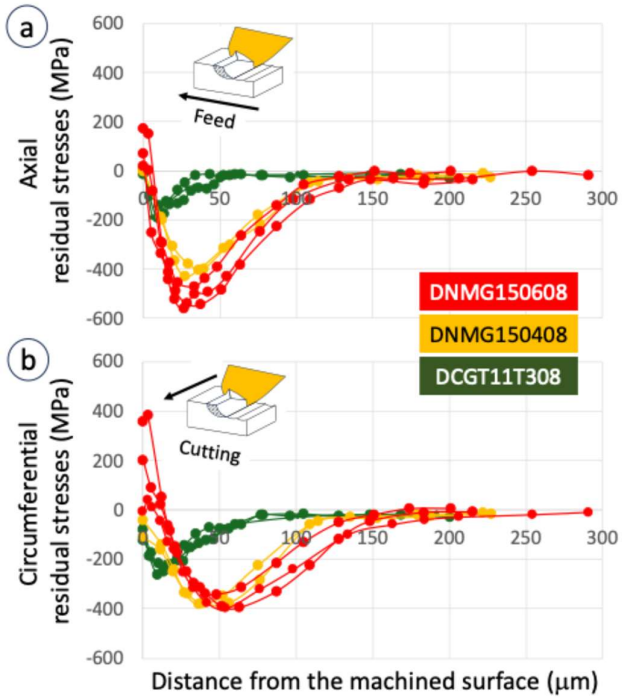

Fig.5. Experimental residual stress states induced by the 3 inserts.

The magnitudes of the residual stress curves differ significantly among the three inserts. The affected depth is directly related to the geometry of the inserts. The roundest tool results in the largest affected depth (120-150µm), whereas the sharpest tool results in the smallest affected depth (50-70µm). This observation is confirmed by the analysis of the average FWHM (Full Width at Half Maximum). The FWHM is provided by the same X-ray diffraction setup (Fig.4). It is quantified by analysing the width of the diffraction peaks. The FWHM correlates with the plastic strain in the material. AS shown in Fig.6, the FWHM for the red and yellow inserts are significantly broader than that of the green insert (sharp edge), indicating that these cutting tools plastically deform the workpiece material to a deeper level.

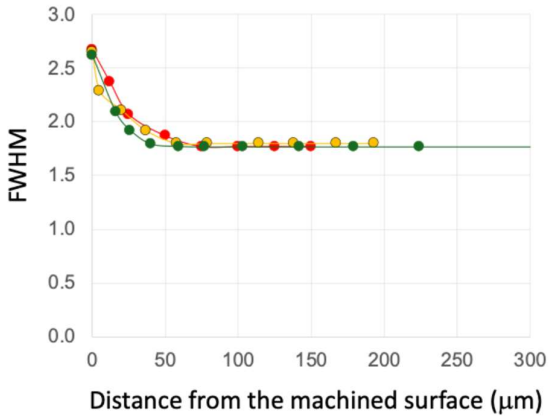

Fig.6. Evolution of the FWHM beneath the machined surface for the three inserts.

This trend regarding the depth of the affected layer has been reported in [6,11,16] during the machining of various metallic alloys. However, their work was limited to a 2D approach involving a single cut on the surface. Investigations restricted to a 2D framework do not reveal that the stress state in the outer layer differs between the axial and circumferential directions. Fig.5 shows that the residual stress state in the outer layer is quite similar for the 3 inserts in the axial direction, while it varies significantly in the circumferential direction. This phenomenon is caused by the interactions of the cutting tool with the previous and subsequent revolutions. Capturing this phenomenon requires simulating multiple revolutions in 3D. The next section will focus on simulating the generation of residual stress in 3D.

Table 3. Residual stress measurement parameters of 15-5PH stainless steel.

Parameter	Value
Diffraction condition	Cr Kα radiation with 20 kV, 4 mA
Wavelength	λ= 0.229 nm
-S1 (v/E)	1.28×10^{-3} GPa^{-1}
S2/2 (1+v)/E	5.92×10^{-3} GPa^{-1}
Plan { h k l }	{ 2 1 1 }
Bragg's angle	$2\theta = 155°$
Beam size	ø2 mm
Polishing strategy	Electropolishing process

3. Numerical modelling

This section aims to simulate the residual stress generated using the MISULAB software [18]. The simulation is based on the "*3D hybrid multi pass model*" developed by [19] and improved by [17] for turning. The prediction of residual stresses is achieved by applying equivalent thermomechanical loadings to a Finite Element (FE) model of the machined surface. The 3D stationary stress distribution is computed through three key steps: 1) decomposing the actual 3D problem into elementary 2D sections, 2) calculating the thermomechanical loadings generated by each section on the machined surface, and 3) simulating the mechanical stress state induced by the merged equivalent loadings after several revolutions, ultimately extracting the residual stress profile at a given location.

3.1. Geometrical decomposition of the 3D problem

The initial step involves decomposing the 3D problem from a geometric standpoint. A geometric model (Fig.7b) is created based on the actual 3D turning configuration (Fig.7a) to identify the relevant cut section (Fig.7c). This cut section may vary according to the tool geometry, tool path and cutting conditions (depth of cut a_p and feed f). The cutting edge is then discretized, and multiple perpendicular cutting planes are established along the cutting zone. These planes define the local tool geometry as well as the corresponding local uncut chip thickness h_i (Fig.7d).

It is crucial to note that the precise tool geometry is considered, which includes the local rake angle γ_n and edge sharpness R_β.

NB: The combination of actual values of local tool geometry, obtained experimentally, with numerical calculations is one of the reasons this approach is termed a "3D *hybrid* muti pass model".

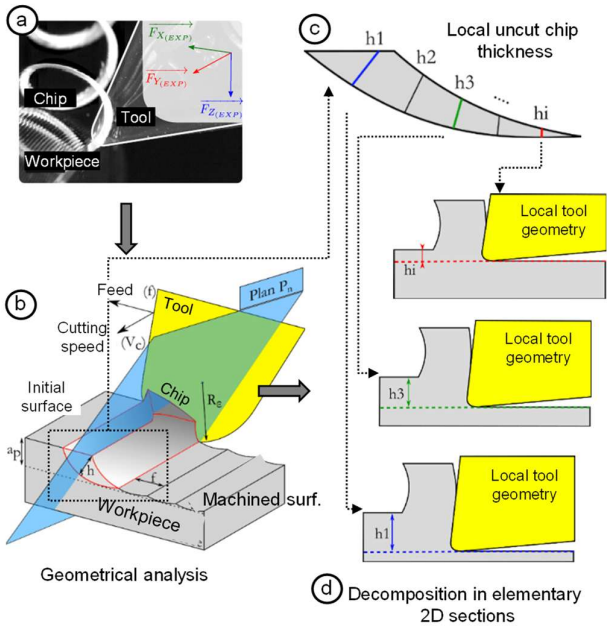

Fig.7. Segmentation procedure of the 3D problem: (a) investigated configuration, (b) geometrical model, (c) identification of the cutting section, (d) decomposition in elementary 2D sections considering the local tool geometry and corresponding uncut chip thickness [15].

3.2. Modelling of the thermomechanical loadings

Each extracted section is subsequently imported into a 2D orthogonal cutting model. 2D thermomechanical simulations are performed within an explicit framework utilizing an Arbitrary Lagrangian-Eulerian (ALE) formulation. A significant advantage of this method is that it enables the separate simulation of each section through parallel computing (Fig.8a).

A Johnson-Cook flow stress model, identified by [19], is used to model the mechanical behaviour of the 15-5 PH steel (Table 4, Eq. 1).

Table 4. Johnson-Cook's parameters of the 15-5 PH

A [MPa]	B [MPa]	n	m	C	$\dot{\varepsilon}_0$	T_F [°C]	T_0 [°C]
855	448	0,14	0.63	0,0137	0.001	1440	20

$$\sigma_{eq} = \left[A + B \cdot \left(\bar{\varepsilon_p}\right)^n\right] \cdot \left[1 + C \cdot \ln\left(\frac{\dot{\varepsilon_p}}{\dot{\varepsilon}_0}\right)\right] \cdot \left[1 - \left(\frac{T - T_0}{T_F - T_0}\right)^m\right] \quad (1)$$

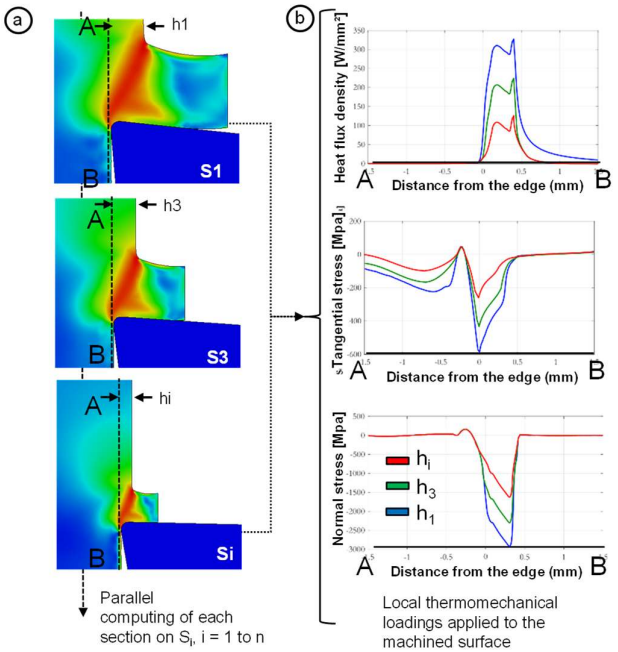

Fig.8. Segmentation procedure of the 3D problem: (a) 2D ALE simulation of each section and (b) extraction of the simulated local thermomechanical loadings withstood by the machined surface [15]

A master (tool) / slave (workpiece) penalty contact method, along with tribologically identified friction and heat partition models, was implemented. The thermal conductance between the tool and the workpiece is 10^4 W/m^2.K.

The interested reader will be able to find all the details and input data in [17,19].

Thermomechanical loadings that the machined surface encounters are obtained along a specific path (A-B, indicated by the dotted black dashed line in Fig.8a), corresponding to the last element layer. The simulations focus on three key outputs: heat flux density, normal stress, and tangential stress variations along this path. Example results for three distinct sections - each representing different local tool geometries and uncut thicknesses - are illustrated in Fig.8b, showing that the magnitude of the three loadings increases with h_i. Lastly, a calibration step is implemented using the machining forces recorded experimentally alongside the combined numerical forces to fine-tune the magnitude of the equivalent thermomechanical loadings [17].

NB: The integration of actual experimentally measured force values with numerical calculations is another reason why this approach is referred to as a "3D *hybrid* muti pass model".

3.3. Simulation of the residual stresses

The 2D loading profiles previously simulated for each section (Fig.8b) are then merged to generate the equivalent 3D thermomechanical loadings (Fig.9a) to be applied in the macroscopic 3D model (Fig.9b). Fig.9b illustrates the resulting loadings, which are then moved along the cutting direction in the FE model according to the cutting speed for a single revolution. Since only an elementary representative volume is modelled, an appropriate cutting time and a consistent cooling phase, accounting for the entire revolution of the workpiece, are calculated and implemented.

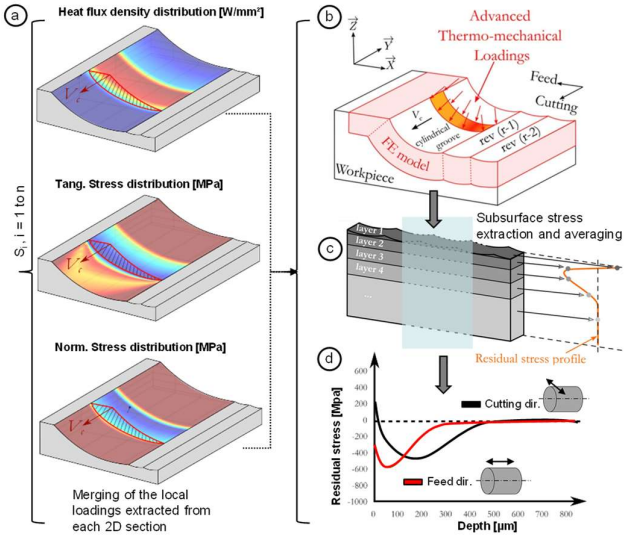

Fig.9. Hybrid simulation method to 3D predict the residual stress distribution: (a) assembling of the 2D loadings to build a 3D loading distribution, (b) implicit 3D FE model with the corresponding loadings, (c) extraction method to generate the stress profile and (d) example of simulated residual stress profiles in the cutting and feed directions [15]

As demonstrated by [17], it is essential to simulate several revolutions to achieve a steady state that considers the interactions of the cutting tool both before and after the cutting zone. Consequently, the model geometry must be updated after every revolution due to material removal. A new geometry of the machined surface and its corresponding mesh are generated, and the residual stress fields are transferred from the previous mesh to the new geometry.

Additionally, to account for the cyclic behaviour of the machined material, a von Mises elastoplastic model with Armstrong-Frederick kinematic hardening is incorporated into this model [19] (Table 5).

Table 5. Coefficients of the Armstrong-Frederick model

Temperature [°C]	*σy [MPa]*	*C*	*γ*
20	530	421.405	730
300	382	284.420	508
600	197	120.000	600

Finally, the numerical residual stresses are extracted layer by layer along the depth and averaged along the feed direction over several revolutions (Fig.9c) to obtain a single residual stress value at each corresponding depth beneath the surface, providing the predicted residual stress profile (Fig.5d).

NB: The simulation of multiple revolutions (multiple successive cuts) is the reason this approach is referred to as a '3D hybrid *multi-pass* model'.

This numerical model is now available in a commercial software called MISULAB. MISULAB is the single simulation software capable of modelling the mechanisms of residual stress generation in 3D while considering a large number of tool passes and calibrating with experimental physical measurements.

3.4. Numerical results

The MISULAB software was used to predict the residual stress states generated by the three cutting tools. The local geometry of the cutting tools was derived from Table 1, while the actual cutting forces, used to calibrate the thermomechanical loadings, were obtained from Table 2. Thus, each simulation for each cutting tool was calibrated independently, taking into account its specific local geometry and its mechanical interaction with the work material.

During the simulations, it was found that simulating at least five revolutions is essential to reach a steady state that accounts for the interactions of the cutting tool both before and after the cutting zone. Simulating five revolutions for a single configuration took 20 hours of CPU time on a 3.2 GHz processor with 4 cores.

Fig.10 displays the simulated gradients of residual stresses induced by the three tools. The results confirm that turning 15-5PH steel generates a typical hook-shaped residual stress profile, characterized by a peak in tensile stress in the outer layer, followed by a compressive peak in the sub-surface. These findings are consistent with previous simulations conducted on similar tools and work materials [17].

Fig.10 shows that the three cutting tools lead to a similar residual stress state in the outer layer. On the contrary, the three cutting tools lead to significantly different residual stress states in the sublayer. The red insert (large edge sharpness R_β and small rake angle γ_n) leads to the largest affected layer with a large compressive state below the surface, while the sharpest tool (green) leads to the smallest. The yellow insert results in an intermediate situation.

3.5. Comparison of experimental and numerical results

Fig.11 compares experimental and numerical residual stress profiles. The comparison reveals that MISULAB predicts the experimental results with reasonable accuracy. The axial residual stress profiles show a good agreement, which highlights that the model takes properly in to account the thermal and mechanical phenomena.

However, for the circumferential residual stresses, it is important to note that the experimental values on the outer surface are quite scattered between -100 and +400 MPa, while the values below the surface are more stable. It is clear that the numerical model does not capture this scattering. The numerical model predicts tensile stresses in the circumferential direction (≈ +400 MPa). The scattering of the experimental results in the narrow external surface may be due to local metallurgical phenomena such as dynamic recrystallisation. The 15-5PH alloy is very much sensitive to this mechanism in turning as shown by [20]. Dynamic recrystallisation occurs within a narrow layer ≈2 µm thanks to the high temperature combined simultaneously with the high plastic deformation. This mechanism leads to a relaxation of the residual stresses. The numerical model does not take this phenomenon into account, which induces an over estimation of the residual stresses in the external layer.

On the contrary, below this disturbed external layer, both experimental and numerical results are very consistent. The model accurately captures the influence of cutting tool geometry. The red tool (large edge sharpness R_β and small rake angle γ_n) produces the largest affected layer (approximately 150 µm), while the sharpest tool (green) results in the smallest affected layer (around 75 µm). The yellow insert exhibits intermediate behavior, with an affected layer of about 100 µm.

Regarding the position and magnitude of the compressive peak, the model confirms that the round tool (red) induces a highly compressive peak deep beneath the surface, whereas the intermediate tool (yellow) has a less significant impact on the subsurface.

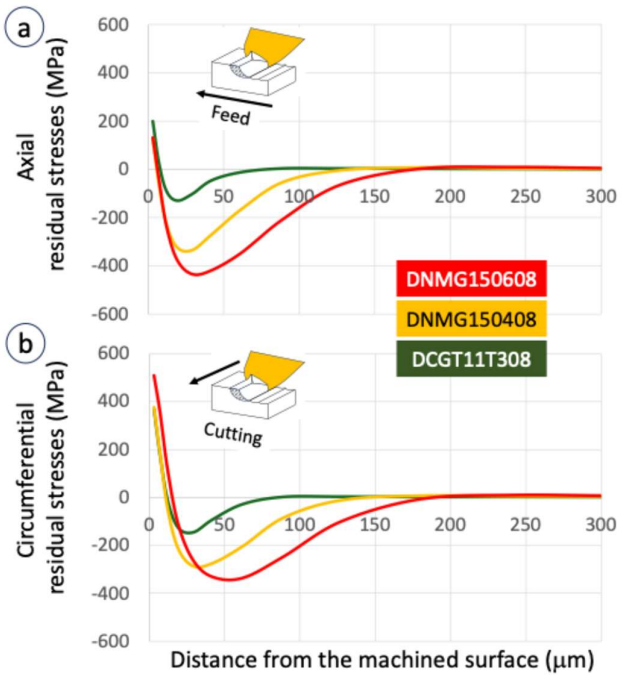

Fig.10. Numerical residual stress profiles induced by the 3 inserts

These findings support the trends observed in previous studies [8, 11], despite their models being primarily 2D and not achieving a steady state after a single revolution. Furthermore, these earlier 2D studies could not demonstrate that the axial residual stress profiles were nearly identical for all three tools, as is consistent with the experimental results.

Overall, these numerical results demonstrate the capability of MISULAB to model the generation of residual stresses in 3D through multi-revolution simulations, calibrated with experimental measurements of actual tool geometry and cutting forces.

4. Conclusions

This study investigates the influence of cutting tool geometry—specifically edge sharpness (Rβ) and rake angle (γn)—on the generation of near-surface residual stresses in 15-5PH martensitic stainless steel. The focus was on the sensitivity of residual stresses to variations in edge sharpness and cutting angle. Three commercially available cutting tools were selected to represent a broad range of these geometric parameters. A dual approach combining both experimental and numerical methods was employed (the '3D hybrid multi-pass model').

The results demonstrate that tools with the smallest edge sharpness (Rβ) and the largest rake angle (γn) effectively limit the affected depth, reduce the magnitude of tensile stresses in the outer layer, and minimize the intensity of the compressive peak in the subsurface. In contrast, the "round" tool (which has high edge sharpness Rβ and a small rake angle γn) induces tensile stresses in the external layer and generates a deeper compressive peak in the subsurface. This trend aligns with findings already documented in the scientific literature. However, this work offers both qualitative and quantitative confirmation of these results through a combined experimental and numerical approach.

Moreover, the study demonstrates that the residual stress generation model, implemented using the MISULAB software, effectively simulates the complex, coupled thermomechanical mechanisms involved in machining. Looking forward, this modeling approach could be leveraged to optimize tool design and cutting conditions, allowing for the precise control of residual stress states tailored to specific applications.

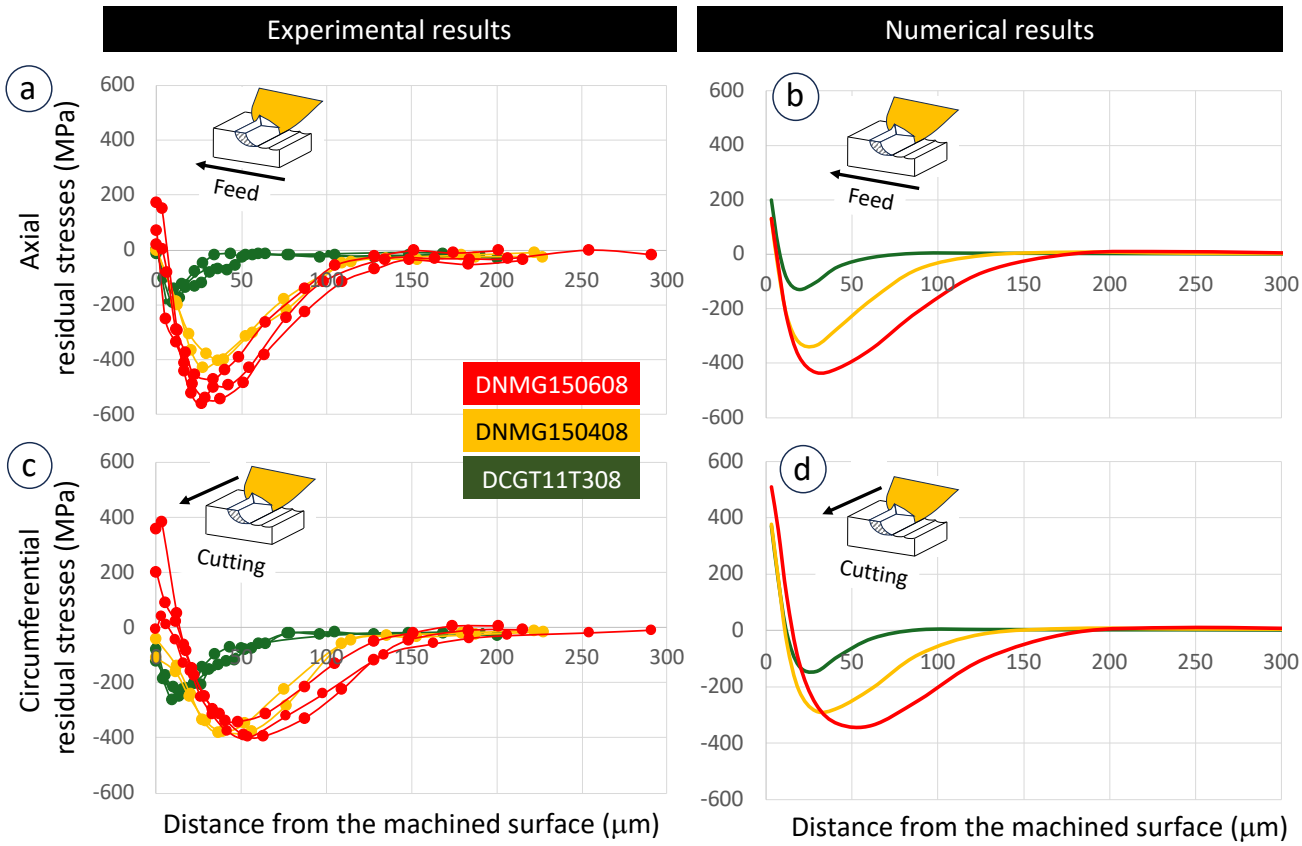

Fig.11. Comparison between experimental and numerical residual stress profiles induced by the 3 inserts

References

[1] Jawahir IS, Brinksmeier E, M'saoubi R, Aspinwall DK, Outeiro JC, Meyer D, Umbrello D, Jayal AD. Surface integrity in material removal processes: Recent advances. CIRP annals 2011; 60-2:603-626.

[2] La Monaca A, Murray JW, Liao Z, Speidel A, Robles-Linares JA, Axinte DA, Hardy MC, Clare AT. Surface integrity in metal machining-Part II: Functional performance. International Journal of Machine Tools and Manufacture 2021;164:103718.

[3] Griffiths B. Manufacturing surface technology: surface integrity and functional performance. London: Prenon Press; 2001.

[4] Rech J, Hamdi, S.Valette, rédaction d'un chapitre dénommé "Surface finish and integrity", Titre de l'ouvrage édité par J. Paulo Davim : « Machining : fundamentals and recent advances », Editions Springer, paru en juillet 2008, XIV, ISBN: 978-1-84800-212-8, pp.59-96

[5] Liu M, Takagi J, Tsukuda A., effect of tool nose radius and tool wear on residual stress distribution in hard turning of bearing stee, Journal of Materials Processing Technologies, 150 (2004) 234-241.

[6] Liu Y, Xu D, Agmell M, M'Saoubi R, Ahadi A, Stahl JE, Zhou J. Numerical and experimental investigation of tool geometry effect on

residual stresses in orthogonal machining of Inconel 718. Simulation Modelling Practice and Theory 2021; 106:102187.
[7] Sharman ARC, Hughes JI, Ridgway K. The effect of tool nose radius on surface integrity and residual stresses when turning Inconel 718. Journal of Materials Processing Technology 2015; 216:123-132.
[8] Huang Z, He S, Kejia Z, Zhang X, Ding H. An analysis of cutting parameters, coated materials, and nose radii on residual stresses when turning Inconel 718. Procedia CIRP 2016; 46:368-371.
[9] Garcia Navas V, Gonzalo O, Bengoetxea I. Effect of cutting parameters on the surface residual stresses generated by turning in AISI 4340 steel. International Journal of Machine Tools and Manufacture 2012; 61:48-57.
[10] Hua J, Umbrello D, Shivpuri R. Investigation of cutting conditions and cutting edge preparations for enhanced compressive subsurface residual stress in the hard turning of bearing steel. Journal of Materials Processing Technology 2006; 171:180-187.
[11] Nasr MNA, Ng EG, Ebestawi MA. Modelling the effects of tool-edge radius on residual stresses when orthogonal cutting 316L. International Journal of Machine Tools & Manufacture 2007; 47:401-411.
[12] Varela PI, Rakurty CS, Balaji AK. Surface integrity in hard machining of 300M steel: effect of cutting edge geometry on machining-induced residual stresses. Procedia CIRP 2014; 13:288-293.
[13] Dahlman P, Gunnberg F, Jacobson M. The influence of rake angle, cutting feed, and cutting depth on residual stresses in hard turning. Journal of Materials Processing Technology 2004; 147:181-184.
[14] Rech J, Moisan A. Surface integrity in finish hard turning of case-hardened steel. International Journal for Machine Tool and Manufacture 2003; 43(5):543-550.
[15] Clavier F, Valiorgue F, Courbon C, Rech J, Van Robaeys A, Chen Y, Kolmacka J, Karaouni H. Towards the numerical simulation of tool wear induced residual stress drift. Procedia CIRP 2024; 123:404-409.
[16] Zong WJ, Sun T, Li D, Cheng K, Liang YC. FEM optimization of tool geometry based on the machined near surface's residual stresses generated in diamond turning. Journal of Materials Processing Technology 2006; 180:271-278.
[17] Dumas M, Fabre D, Valiorgue F, Kermouche G, Van Robaeys A, et al. 3D numerical modelling of turning-induced residual stresses – A two-scale approach based on equivalent thermo-mechanical loadings. Journal of Materials Processing Technology 2021; 297:117274.
[18] https://www.misulab.fr
[19] Mondelin A, Valiorgue F, Rech J, Coret M, Feulvarch E. Hybrid model for the prediction of residual stresses induced by 15-5PH steel turning. International Journal of Mechanical Sciences 2012; 58(1):69
[20] Dumas M, Valiorgue F, Kermouche G, Van Robaeys A, Masciantonio, U, Brosse A, Karaouni H, Rech, J. Evolution of the surface integrity while turning a fillet radius in a martensitic stainless steel 15-5PH. Procedia CIRP 2020; 87:101-106